Influence of the Elastic Dilatation of Mining-Induced Unloading Rock Mass on the Development of Bed Separation

Authors:

Weibing Zhu, Shengchao Yu, Jingmin Xu

Date Submitted: 2020-06-23

Keywords: bed separation, super-thick igneous rock, mining-induced rock mass, key stratum, unloading dilatation

Abstract:

Understanding how mining-induced strata movement, fractures, bed separation, and ground subsidence evolve is an area of great importance for the underground coal mining industry, particularly for disaster control and sustainable mining. Based on the rules of mining-induced strata movement and stress evolution, accumulative dilatation of mining-induced unloading rock mass is first proposed in this paper. Triaxial unloading tests and theoretical calculation were used to investigate the influence of elastic dilatation of mining-induced unloading rock mass on the development of bed separation in the context of district No. 102 where a layer of super-thick igneous sill exists in the Haizi colliery. It is shown that the elastic dilatation coefficient of mining-induced unloading hard rocks and coal were 0.9~1.0‰ and 2.63‰ respectively under the axial load of 16 MPa, which increased to 1.30~1.59‰ and 4.88‰ when the axial load was 32 MPa. After successively excavating working faces No. 1022 and No. 1024, the elastic dilatation of unloading rock mass was 157.9 mm, which represented approximately 6.3% of the mining height, indicating the elastic dilatation of mining-induced unloading rock mass has a moderate influence on the development of bed separation. Drill hole detection results after grouting, showed that only 0.33 m of the total grouting filling thickness (1.67 m) was located in the fracture zone and bending zone, which verified the result from previous drill hole detection that only small bed separation developed beneath the igneous sill. Therefore, it was concluded that the influences of elastic dilatation of mining-induced unloading rock mass and bulking of caved rock mass jointly contributed to the small bed separation space beneath the igneous sill. Since the accurate calculation of the unloading dilatation of rock mass is the fundamental basis for quantitative calculation of bed separation and surface subsidence, this paper is expected to be a meaningful beginning point and could provide a useful reference for future, related research.

Record Type: Published Article

Submitted To: LAPSE (Living Archive for Process Systems Engineering)

Citation (overall record, always the latest version):	LAPSE:2020.0740
Citation (this specific file, latest version):	LAPSE:2020.0740-1
Citation (this specific file, this version):	LAPSE:2020.0740-1v1

DOI of Published Version: https://doi.org/10.3390/en11040785

energies

MDPI

Article

Influence of the Elastic Dilatation of Mining-Induced Unloading Rock Mass on the Development of Bed Separation

Weibing Zhu [1,2], Shengchao Yu [1] and Jingmin Xu [3,*]

1 Key Laboratory of Deep Coal Resource Mining, Ministry of Education of China; School of Mines, China University of Mining and Technology, Xuzhou 221116, China; zweibing@163.com (W.Z.); yushengchao@cumt.edu.cn (S.Y.)
2 State Key Laboratory of Coal Resource and Safe Mining, China University of Mining and Technology, Xuzhou 221116, China
3 Department of Civil Engineering, Faculty of Engineering, University of Nottingham, University Park, NG7 2RD Nottingham, UK
* Correspondence: jingmin.xu@nottingham.ac.uk

Received: 6 January 2018; Accepted: 27 March 2018; Published: 29 March 2018

Abstract: Understanding how mining-induced strata movement, fractures, bed separation, and ground subsidence evolve is an area of great importance for the underground coal mining industry, particularly for disaster control and sustainable mining. Based on the rules of mining-induced strata movement and stress evolution, accumulative dilatation of mining-induced unloading rock mass is first proposed in this paper. Triaxial unloading tests and theoretical calculation were used to investigate the influence of elastic dilatation of mining-induced unloading rock mass on the development of bed separation in the context of district No. 102 where a layer of super-thick igneous sill exists in the Haizi colliery. It is shown that the elastic dilatation coefficient of mining-induced unloading hard rocks and coal were 0.9~1.0‰ and 2.63‰ respectively under the axial load of 16 MPa, which increased to 1.30~1.59‰ and 4.88‰ when the axial load was 32 MPa. After successively excavating working faces No. 1022 and No. 1024, the elastic dilatation of unloading rock mass was 157.9 mm, which represented approximately 6.3% of the mining height, indicating the elastic dilatation of mining-induced unloading rock mass has a moderate influence on the development of bed separation. Drill hole detection results after grouting, showed that only 0.33 m of the total grouting filling thickness (1.67 m) was located in the fracture zone and bending zone, which verified the result from previous drill hole detection that only small bed separation developed beneath the igneous sill. Therefore, it was concluded that the influences of elastic dilatation of mining-induced unloading rock mass and bulking of caved rock mass jointly contributed to the small bed separation space beneath the igneous sill. Since the accurate calculation of the unloading dilatation of rock mass is the fundamental basis for quantitative calculation of bed separation and surface subsidence, this paper is expected to be a meaningful beginning point and could provide a useful reference for future, related research.

Keywords: unloading dilatation; key stratum; bed separation; super-thick igneous rock; mining-induced rock mass

1. Introduction

Coal seam excavation induces the movement of overlying strata, which can be divided into three zones; the caving zone, fracture zone and bending zone from the immediate roof upwards according to the degree of failure of the overburden [1–4]. The development of the three zones is closely related

to mining ground pressure [5,6], mining-induced fractures [7], bed separation [8] as well as surface subsidence [9,10]. Coal mining is an unloading process of the rock mass from an original stress state, which inevitably results in bed separation due to the out-of-step movement of the unloading strata [11]. Many scholars have conducted in-depth study on the generation mechanism, position as well as size of bed separation, and they have proposed various bed separation identification methods [12–16]. Xuan et al. [17] applied the technology, isolated grout injection into dynamic bed separation in the overburden under mining conditions, to control the surface subsidence and ensure the safety of the buildings in the village at the surface. Xing et al. [18] proposed the mechanism of water-inrush and its preventative measures based on the water-inrush accidents resulting from water accumulation at the bed separation zone in the mining overburden. Under the circumstance of dewatering and danger of flooding resulting from mining and mining-induced subsidence, a prediction for the optimization of drive-in filters was applied to ensure mining safety [19].

The key stratum theory [20], which indicates that the key strata can be used to control the movement of part or of an entire strata, has been used frequently in the study of strata movement and control, as well as a method to determine the location of key stratum in overlying strata [2,9]. Bed separation mainly occurs below each key stratum, and its size depends on the mining height, the total bulking increment of rock mass under the key stratum and the deflection of the corresponding key stratum [21]. It is generally believed that the bulking increment generated by the caved gangue in the caving zone dominates the total bulking increment of rock mass beneath the key stratum, and therefore it has been extensively studied by many researchers [22–26]. By the use of self-designed loosing and compacting equipment, Miao et al. [22] investigated the bulking factor, bulking curve, compaction curve and pressure-measuring curve of rock and coal samples with a grain size smaller than 11.3 mm as a function of compression stress. Guo et al. [23] studied bulking and compacting properties of broken rock mass in the goaf, and pointed out the distribution of bulking factors for broken rock mass in the longwall goaf. Jiang et al. [24], based on their study on the mechanism of the gangue's breakage and compaction, concluded that the progressive compacting procedure of the gangue could be divided into two stages, with the former known as breakage compaction, while the latter is known as concretion compaction. Salamon [25] obtained the stress-strain relationship of caved rock mass in research on the deformation properties of broken rock mass. Su et al. [26] analyzed the effect of the rock strength, block size and compression stress on the compaction properties of broken roof rock by conducting compaction test using self-designed equipment. All of these studies aimed to investigate the laws of bulking and compacting of broken rock mass in the caving zone and have provided crucial references for strata movement analysis, bed separation and surface subsidence prediction. Although the broken strata in the fracture zone and the bending zone do not have bulking properties similar to the caved rock blocks in the caving zone, they are also subject to different stress changes as a result of mining-induced unloading. The bulking volume generated in a single stratum caused by unloading could be negligible, however, the accumulated bulking volume of entire strata beneath the key stratum cannot be neglected. Particularly in the case where the mining depth is deep and the distance from the primary key stratum (the key stratum that controls the entire strata from itself up to the ground surface) to the coal seam is far, both the thickness of the unloading strata and the unloading value are large, so that the bulking volume in the fracture zone and bending zone may have an important impact on the development of bed separation. However, there has not been relevant research on this issue to the best knowledge of the authors.

Thus, this paper aims to investigate the above-mentioned issue based on the typical geological conditions in the Haizi coal mine, which contains super-thick igneous sill. The accumulative dilatation effect of mining-induced unloading rock mass is first proposed. This is followed by a description of the geological site of this research. The accumulated dilatation of the rock mass beneath the key stratum can be calculated after the determination of the unloading dilatation coefficient obtained from the triaxial test. Furthermore, the effect of the elastic dilatation of mining-induced unloading rock mass

on the development of bed separation in the Haizi coal mine was evaluated combined with a grout injection project. Finally, the limitations of this research are discussed and further work is suggested.

2. Accumulative Dilatation of Mining-Induced Unloading Rock Mass

Coal seam excavation induces the movement of overlying strata, and according to the degree of failure [1–4], the overlying strata can be divided into three zones from the immediate roof to the surface, namely, the caving zone, fracture zone and bending zone as shown in Figure 1. In general, the large bulking dilatation of broken rock mass in the caving zone has gained widespread attention by previous researchers [22–26]. However, the rock mass in the fracture zone and bending zone also undergo unloading although without being fully crushed. The bulking volume generated in a single stratum caused by unloading may be negligible, but the accumulated bulking volume of entire strata beneath the key stratum cannot be neglected, as it may have an important impact on the development of bed separation.

As shown in Figure 1, the area from the upper boundary of the caving zone to the lower boundary of the unbroken key stratum is defined as the unloading dilatation zone. The strata within this area are subject to a mining-induced unloading effect so that (elastic) dilatation occurs. The accurate calculation of the unloading dilatation of rock mass is the fundamental basis for the quantitative calculation of bed separation beneath the unbroken key stratum.

It is clear that if the mining depth is deep and the distance from the primary key stratum to the coal seam is far, both the thickness of the unloading strata and the unloading value are large, and this would result in a considerable amount of unloading dilatation. The Haizi coal mine possesses special geological conditions featuring super-thick igneous sill and it is deeply buried, which provides a favorable context for this research. Thus, the research for this paper is mainly based on the Haizi coal mine.

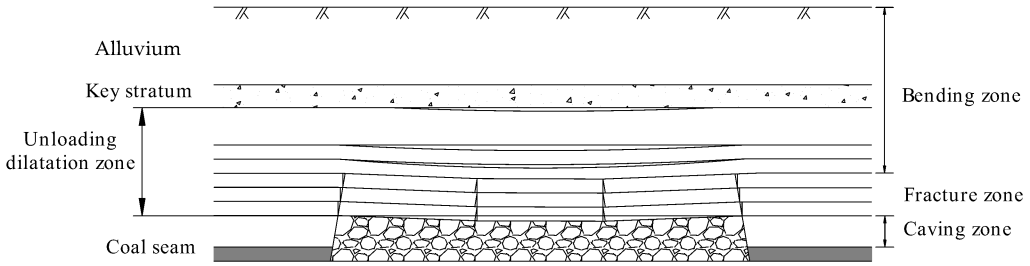

Figure 1. Diagram of three zones division.

3. Site Description

Haizi coal mine, located at Huaibei in Anhui Province in China, belongs to the Huaibei Mining Co. Ltd. (Huaibei, China), and has exploited since 1978 The location of the mine can be seen in Figure 2. The No. 102 district in the Haizi coal mine, which develops coal seam No. 10, has two wings with the average thickness and average inclination of the coal seam being approximately 2.5 m and 18° respectively, and a mining depth in the range from 587 m to 737 m. The west wing of this district includes three working faces, No. 1022, No. 1024 and No. 1026, as shown in Figure 3. With No. 1022 and No. 1024 being exploited in succession, the slope distance of these two working faces has accumulated over 390 m and the advancement distance is around 560 m. The average thickness of the loose bed is 240 m, and the igneous sill was found beneath the loose bed with around 170 m distance to the coal seam. The igneous rock is distributed evenly with an average thickness of about 140 m, and therefore it was regarded as super-thick igneous sill, as shown in Figure 4. Considering that the average mining depth is 627 m and the thickness of the loose bed is 240 m, it was concluded that the full-mining stage had been achieved. However, the maximal surface subsidence was measured at only around 500 mm [8], which indicates that the super-thick igneous sill acts as the primary key stratum and is

unbroken. Although district No. 102 is buried deeply, the super-thick igneous sill bears the load of the 400 m-thick overlying strata, which helps the underlying coal and rock strata, which has a thickness of up to 180 m, to fully unload.

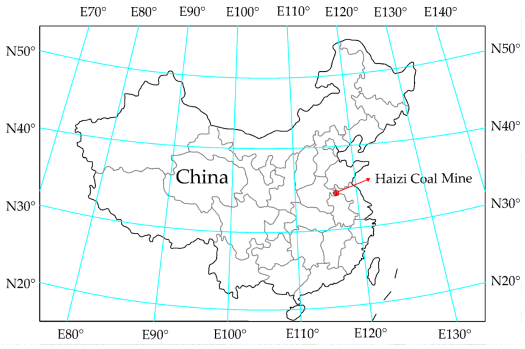

Figure 2. Location of Haizi coal mine.

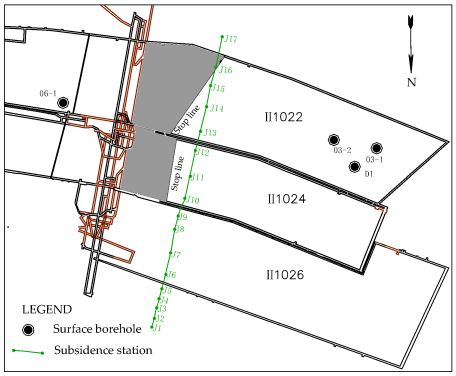

Figure 3. Plan view of the west wing of district No.102.

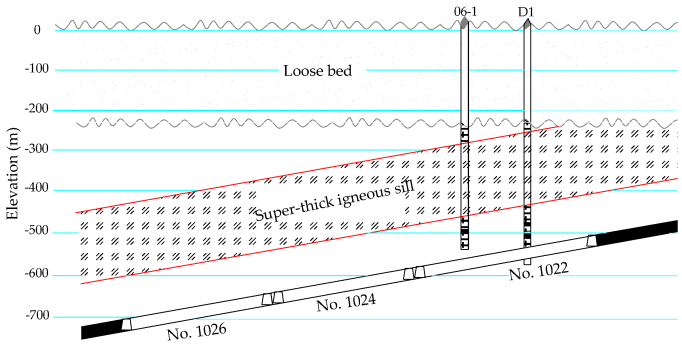

Figure 4. Cross-sectional view of the west wing of the district No.102.

4. Determining the Unloading Dilatation Coefficient in the Laboratory

In order to quantitatively analyze the unloading dilatation of rock mass, representative rocks [27] in the overlying strata of district No. 102 were selected to carry out the loading-unloading test. Once the unloading dilatations of various types of rocks were determined, the accumulated unloading dilation of the strata under the igneous sill can then be calculated.

4.1. Experimental Equipment and Rock Specimens Preparation

All the samples came from drill hole 06-1 in district No. 102, as shown in Figure 4. This drill hole is approximately located in the center of district No. 102 so that it can provide a good representation

of the actual geological condition. Five types of standard test specimens, namely, coarse sandstone, igneous rock, sand-shale, bauxite and coal, were prepared, as shown in Figure 5. Based on the geologic column in Figure 6, only the above-mentioned five types were preserved -due to limitations in the number of drill holes and the difficultly of coring. Therefore, they became the fundamental basis for this experiment.

Figure 5. Five types of specimens.

No.	*T* (m)	*H* (m)	Lithology	Columnar					
1	243.00	243.00	Alluvium						
2	2.27	245.27	Sandstone						
3	6.01	251.28	Siltstone						
4	15.76	267.04	Packsand						
5	1.77	268.81	Siltstone		39	1.74	563.30	Packsand	
6	9.16	277.97	Sandshale		40	0.26	563.56	Seam	
7	4.28	282.25	Siltstone		41	7.60	571.16	Siltstone	
8	6.06	288.31	Packsand		42	1.84	573.00	Packsand	
9	0.98	289.29	Siltstone		43	1.26	574.26	Sandshale	
10	2.17	291.46	Sandstone		44	1.35	575.61	Packsand	
11	2.95	294.41	Sandshale		45	2.12	577.73	Siltstone	
12	2.76	297.17	Sandshale		46	3.20	580.93	Sandshale	
13	19.80	316.97	Magmatite		47	3.44	584.37	Sandshale	
14	5.22	322.19	Sandshale		48	7.65	592.02	Packsand	
15	136.10	458.29	Magmatite		49	4.21	596.23	Sandshale	
16	16.82	475.11	Siltstone		50	0.96	597.19	Siltstone	
17	2.91	478.02	Packsand		51	0.86	598.05	Packsand	
18	1.22	479.24	Siltstone		52	2.10	600.15	Siltstone	
19	10.43	489.67	Sandstone		53	1.72	601.87	Sandshale	
20	13.29	502.96	Sandshale		54	1.90	603.77	Siltstone	
21	0.23	503.19	Seam		55	1.24	605.01	Packsand	
22	1.74	504.93	Sandshale		56	11.49	616.50	Siltstone	
23	3.25	508.18	Siltstone		57	5.92	622.42	Sandstone	
24	2.60	510.78	Sandshale		58	3.16	625.58	Siltstone	
25	4.19	514.97	Siltstone		59	1.93	627.51	Sandstone	
26	2.87	517.84	Sandstone		60	4.44	631.95	Siltstone	
27	0.67	518.51	Packsand		61	1.45	633.40	Packsand	
28	1.18	519.69	Sandshale		62	2.22	635.62	Siltstone	
29	1.94	521.63	Seam #7		63	1.84	637.46	Packsand	
30	18.05	539.68	Sandshale		64	3.57	641.03	Sandshale	
31	1.58	541.26	Packsand		65	2.70	643.73	Packsand	
32	0.57	541.83	Sandshale		66	0.55	644.28	Siltstone	
33	4.11	545.94	Siltstone		67	3.10	647.38	Seam #10	
34	8.58	554.52	Packsand		68	0.74	648.12	Sandshale	
35	0.92	555.44	Seam #8		69	0.68	648.80	Seam	
36	1.60	557.04	Sandshale		70	4.60	653.40	Siltstone	
37	1.14	558.18	Seam #9		71	3.81	657.21	Packsand	
38	3.38	561.56	Sandshale		72	8.69	665.90	Siltstone	

Figure 6. Columnar section of drill hole 06-1. *T* is the thickness of each stratum. *H* is the distance from each stratum to ground.

The electro-hydraulic servo rock testing system MTS815 at the Skate Key Laboratory for Geomechanics and Deep Underground Engineering, CUMT was used to conduct the test. It was a multifunctional electro-hydraulic servo controlled rigidity machine specialized in testing rock and concrete. The experimental system consists of a loading system, controller and measuring system, etc. Stress control was selected to apply both the lateral and axial load during the tests.

4.2. Experiment Schemes

Identifying and calculating both vertical and horizontal stresses are very complicated due to the coal mining being underground, especially if the conditions are influenced by tectonic stress. The authors attempted to numerically simulate the stress change of the rock mass due to longwall mining. The results showed that the stresses, especially for the horizontal stress of the rock mass, were very complicated and the variation in the stresses within the rock mass in different positions were entirely different, although tectonic stress was ignored (i.e., only considering Hooke's law). It was concluded that reproducing the realistic stress path of the rock mass in the laboratory experiment was unpractical. Therefore, the stress path was simplified in this paper.

The average mining depth of district No. 102 in Haizi coal mine is around 627 m. Since, without considering the influence of tectonic stress, the vertical stress was theoretically calculated to be 15.67 MPa with the average unit weight evaluated as 25 KN/m^3, as such, the axial load in the experiment was chosen as 16 MPa. Meanwhile, in order to make a comparison, an axial load of 32 MPa was applied in another test to simulate the deeper mining. According to Hooke's law, the coefficient of lateral load can be calculated as $\mu/(1-\mu)$, considering that the Poisson's ratio of rock ranged from 0.2 to 0.3, the coefficient of lateral load was calculated to be 0.25–0.43. Without considering the influence of tectonic stress, the horizontal stress was calculated to be 4–6.4 MPa when the axial load was 16 MPa, thus the lateral load in the experiment was selected to be 5 MPa. The lateral load was 10 MPa when the axial load was 32 MPa. The final coefficient of lateral load was 0.31.

With the excavation of coal resources, unloading occurred in the overlying strata layer by layer. The stress in the vertical direction is relieved initially and is then followed by the relief of the horizontal stress due to the bending of the strata. According to the general unloading rules of the stress in each direction for unloading rock mass in dilatation areas, experimental schemes were formulated as follows: (1) Since the rock mass has experienced replicated loading and unloading in the diagenesis process, the rock specimens underwent loading and unloading twice to achieve the original stress state in situ, as far as possible. The axial load and lateral load were increased from zero to the maximum at the same rate, after which the lateral load was kept stable, while the axial load decreased to the same value as the lateral load before it increased to the maximum again; (2) In the process of unloading, the axial load was decreased to the same value as the initial lateral load, then both the lateral and axial loads were reduced to zero swiftly and at the same time. The stress paths in the triaxial test with two different types of the maximal axial load are illustrated in Figure 7. The rate of both loading and unloading for the axial and lateral loads in this experiment was 0.1 MPa/s.

All the specimens were sealed prior to loading. The stress-strain curves for axial direction, lateral direction and volume of rock specimens were recorded during the test, as shown in Figure 8.

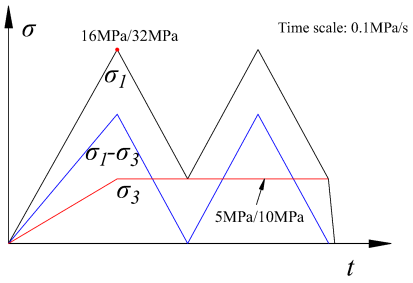

Figure 7. Stress paths used for the experiment.

Figure 8. All the procedures used for the experiment.

4.3. Test Results and Analysis

Since the rock unloading dilatation coefficient in the axial direction had the closest relationship with the development of bed separation, only the axial test results are shown in this paper. Additionally, as the deformation behaviors and dilatation coefficients of hard rocks (coarse sandstone, igneous rock, sand shale and bauxite) were almost identical, only the deviatoric stress-axial strain curves of the coarse sandstone are discussed in this study due to space limitations. The results were then compared to that of the coal specimen. The test results with an axial load of 16 MPa and 32 MPa are shown in Figures 9 and 10, respectively.

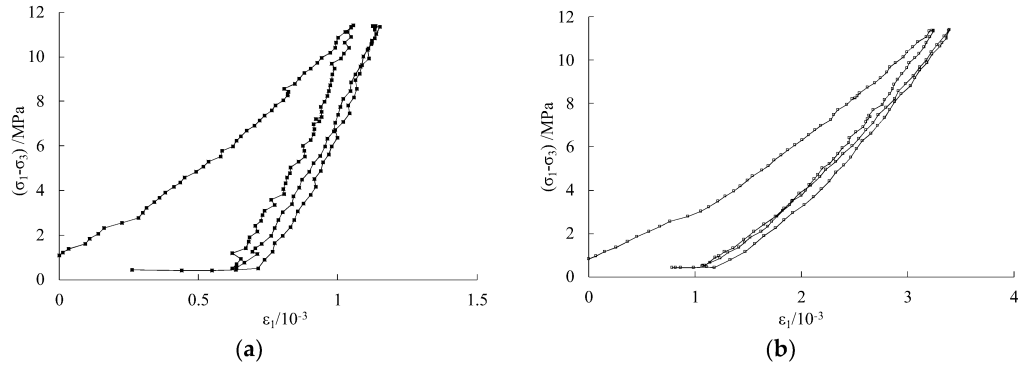

Figure 9. Deviatoric stress-axial strain curves of different specimens under low stress: (**a**) Coarse sandstone; (**b**) Coal.

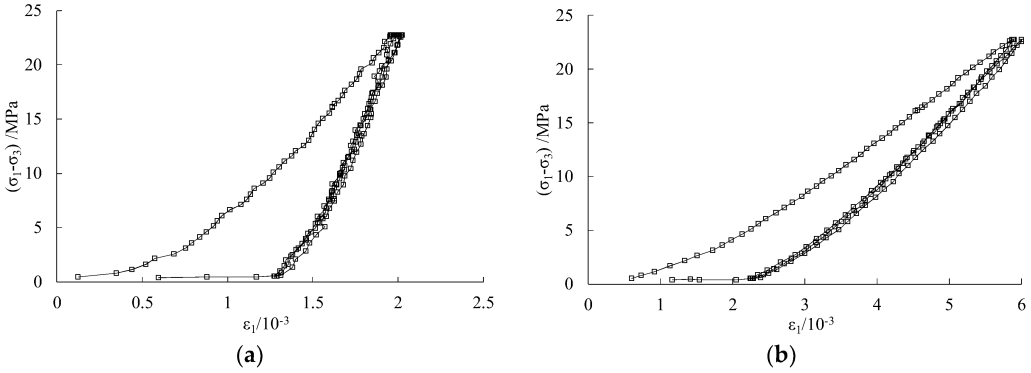

Figure 10. Deviatoric stress-axial strain curves of different specimens under high stress: (**a**) Coarse sandstone; (**b**) Coal.

The deviatoric stress-axial strain curves of specimens can be drawn as shown in Figure 11 according to experimental results. By analyzing the deviatoric stress-axial strain curves of different specimens in Figures 9 and 10, it can be concluded that:

(1). In section A–B of Figure 11 where the deviatoric stress was increased to the peak for the first time, both curves for coal and hard rock showed an uptrend tendency with the deviatoric stress increasing, and the slope of the curves keeps increasing, which indicates that the fractures in the specimens gradually closed as the stress grew. At lower stress, the hard rock was at the fracture compacting stage while the coal experienced the fracture compacting stage at first and then underwent elastic deformation. The hard rock experienced elastic deformation at higher stress. This is due to the hardness difference between coal and hard rock. The coal was relatively soft compared with hard rock, and its micro fractures were closed under a low stress state while high stress was need to close the micro fractures in hard rock.

(2). Sections B–C, C–D and D–E in Figure 11 refer to the stage during which the sample experienced repeated axial loading and unloading while the lateral load remained stable. It can be seen that the loading and unloading curves for coal and hard rock were not smooth at low stress, which is similar to the early loading stage characterized as faint fracture compaction. When the deviatoric stress decreased to zero and then increased again, the deviatoric stress-axial strain curve did not overlap with the last unloading curve. There is a slight deviation existing in the two curves, which is due to the fracture compacting and then opening under a low stress state. Under a high stress state, the loading and unloading curves of coal and hard rock are smooth, and there is a high level of overlap between the second loading curve and the first unloading curve, indicating that almost all the fractures were closed and the specimen was in a nearly perfect elastic state when the stresses in all the three directions were 10 MPa.

(3). In the later section E–F, both the lateral and axial loads were quickly reduced to zero to ensure the deviatoric stress was equal to zero, helping the specimens to achieve full unloading. Note that neither the coal nor the hard rock recovers their full strain value, this was because the energy, stored in the micro-fracture after loading, was not completely relieved. The dilatation coefficients of the four types of hard rocks were generally identical, and that of coal was two to three times larger, which indicates that the mining-induced unloading had more significant influence on the dilatation coefficient of coal.

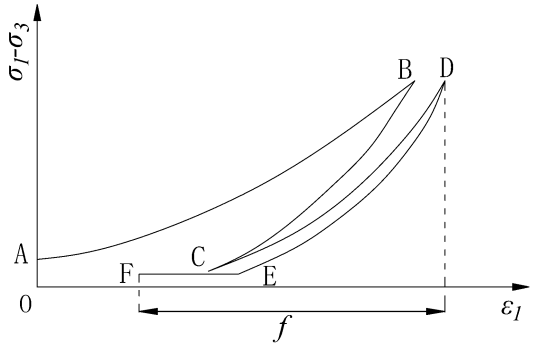

Figure 11. Schematic diagram showing the deviatoric stress-axial strain curves of different specimens.

4.4. Calculation of the Unloading Elastic Dilatation Coefficient

Elastic dilatation occurs when the strata at original stress state is influenced by mining-induced unloading. Provided that the initial thickness of a stratum is h_1 and the thickness after unloading is h_2, the unloading elastic dilatation coefficient, f can be determined using Equation (1):

$$f = \frac{h_2 - h_1}{h_1} \quad (1)$$

If the data in this experiment were used to make the calculation, then f would be determined using Equation (2):

$$f = \frac{h_2 - h_1}{h_1} = \frac{h_0(1-\varepsilon_F) - h_0(1-\varepsilon_D)}{h_0(1-\varepsilon_D)} = \frac{\varepsilon_D - \varepsilon_F}{1-\varepsilon_D} \quad (2)$$

where h_0 is the initial height of the specimens, ε_D and ε_F are the lateral strains at position D and position F, respectively as shown in Figure 11.

Substituting the experimental data into Equation (2) produces the elastic dilatation coefficients of four unloading hard rocks and coal at low and high stresses, as shown in Table 1.

Table 1. Different specimens unloading dilatation coefficients in the experiment.

Stress	Coarse Sandstone	Bauxite	Igneous Rock	Sandshale	Coal
16 MPa	0.90‰	0.97‰	0.92‰	0.91‰	2.63‰
32 MPa	1.42‰	1.30‰	1.59‰	1.43‰	4.88‰

The elastic dilatation coefficients of mining-induced unloading rock mass at low and high stresses are shown in Table 1. It is clear that, when the axial load is 16 MPa and the lateral load is 5 MPa, apart from the coal which has a slightly larger elastic dilatation coefficient of 2.63‰, the elastic dilatation coefficients of the hard rocks are in the range from 0.9‰ to 1.0‰, which indicates that different rocks have approximately the same dilatation coefficient at identical cover depth. When the axial and lateral loads were increased to 32 MPa and 10 MPa respectively, the elastic dilatation coefficients of the hard rocks also increased, being 1.3‰ to 1.59‰, respectively, which demonstrates that the elastic dilatation coefficients of mining-induced unloading rock mass increases with the cover depth, but still at a small level. It is apparent that there is a great difference between the elastic dilatation coefficient of mining-induced unloading rock mass and the bulking factor of caved rock mass in the caving zone, and the latter generally reaches over 20% in the earlier caving stage even though the residual bulking factor was still over 3%, which illustrates that the elastic dilatation coefficient of unloading rock mass is much smaller than the bulking factor of the fractured rock in the caving zone and they are not at the same order of magnitude.

5. Calculation of the Accumulated Elastic Dilatation of Unloading Rock Mass

The unloading elastic dilatation coefficient measured in the triaxial test was used to calculate the accumulated dilatation of unloading rock mass beneath the igneous sill in the west wing of district No. 102 in the Haizi coal mine. Due to the limited number of drill hole coring, not all of the rocks were tested in this study, for example, medium coarse sandstone and pack-sand. However, as indicated by the results of laboratory tests on rock samples, the medium coarse sandstone and pack-sand have nearly similar unloading elastic dilatation coefficients to coarse sandstone, and there was only a slight difference of 0.01‰ in the unloading elastic dilatation coefficient between coarse sandstone and sand-shale no matter if under a state of high or low stress, the difference was also slight when it came to igneous rock with higher hardness. Thus, in this study, the unloading elastic dilatation coefficient of all the sandstones was selected as 0.90‰ and 1.42‰ at low and high stresses, respectively. It is necessary to note, that all specimens were placed in a state of 16 MPa or 32 MPa in the triaxial test, which is probably not equal to the actual in situ stress of the rock mass. The associated effect on the calculation results is discussed later.

According to the geologic column of drill 06-1, the accumulated unloading dilatation of various lithological strata was calculated using the unloading elastic dilatation coefficients measured in the tests, as shown in Table 2.

Table 2. Total amount of unloading dilatation with different lithology.

Lithology	Accumulated Thickness/m	16 MPa		32 MPa	
		Dilatation Coefficient	Dilatation/mm	Dilatation Coefficient	Dilatation/mm
Coarse sandstone	7.85	0.90‰	7.1	1.42‰	11.1
Sandshale	56.37	0.91‰	51.3	1.43‰	80.6
Bauxite	3.44	0.97‰	3.3	1.30‰	4.5
Medium sandstone	13.3	0.90‰	12.0	1.42‰	18.9
Packsand	34.67	0.90‰	31.2	1.42‰	49.2
Siltstone	65.58	0.90‰	59.0	1.42‰	93.1
Coal	4.23	2.63‰	11.1	4.88‰	20.6
Total	185.44	/	175.0	/	278.0

According to Table 2, the 185.44 m thick coal and rock strata beneath the super-thick igneous sill in district No. 102 has an accumulated dilatation of 175 mm after fully unloading. The elastic dilatation increased to 278 mm when the mining depth doubled. Thus, the accumulated unloading dilatation of the same thick strata magnifies with an increase in the mining depth and it can be concluded that the accumulated unloading dilatation is proportional to the mining depth.

However, although the super-thick igneous sill did not break, the underlain 185.44 m thick coal and rock strata would be pressed by the gravity of the overburden. As it was not practical to test the unloading dilatation coefficients with various cover depths, theoretical calculation was employed to estimate the reduction in dilatation of unloading rock mass due to pressure induced by overburden, and theoretical calculation was further used to determine the actual dilatation of the unloading rock mass beneath the igneous sill after the excavation of working faces No. 1022 and No. 1024 in district No. 102.

When the rock mass is loaded with the stress, σ_1 in a vertical direction by the overburden, assuming the lateral deformation is restricted, a lateral load $\mu\sigma_1$ would be produced according to the hydrostatic pressure theory, where μ is the Poisson's ratio. A cell cube was extracted from the rock mass as a typical example with its stress state shown in Figure 12.

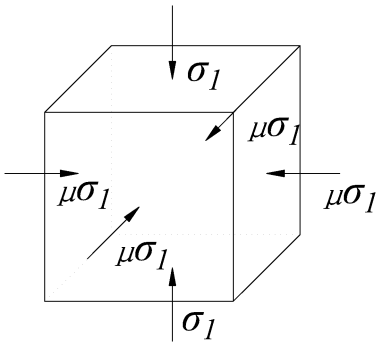

Figure 12. Schematic diagram of the stress in the unit.

Assuming the number of all the strata layers between the igneous sill and the caving zone is m, and the load transfer coefficient is deemed as 1, then the compressibility, Δh_i of the stratum No. i resulting from the compression induced by the upper '$m - i$' layers of strata could be determined with Equation (3):

$$\Delta h_i = \frac{h_i \sum_{j=i+1}^{m} \gamma_j h_j}{E_i} \left(1 - \frac{2\mu_i^2}{1 - \mu_i}\right) \quad (3)$$

where h_i is the depth of the stratum i after fully unloading, γ_i & μ_i are the average unit weight and the Poisson's ratio of the stratum i, respectively.

The internal compressibility, S of unloading rock mass can be determined with Equation (4):

$$S = \sum_{i=1}^{m} \Delta h_i = \sum_{i=1}^{m} \frac{h_i \sum_{j=i+1}^{m} \gamma_j h_j}{E_i} \left(1 - \frac{2\mu_i^2}{1-\mu_i}\right) \quad (4)$$

Parameters gained from tests on rock core in the columnar section of drill hole 06-1 were substituted in Equation (4), the total compressibility of unloading rock mass due to the existence of internal load was calculated to be 17.1 mm. Then, the accumulated dilatation of mining-induced unloading rock mass beneath the igneous sill after the excavation of working faces No. 1022 and No. 1024 in district No. 102 was calculated to be 157.9 mm. This suggested that the elastic dilatation of mining-induced unloading rock mass beneath the super-thick igneous sill was small and as such would have only a slight influence on the development of bed separation.

6. Engineering Verification

After the successive excavation of working faces No. 1022 and No. 1024, full mining was achieved. According to the subsidence data of the nearby Linhuan coal mine and Tonglin coal mine, the coefficient of surface subsidence is about 1 at the full-mining stage. However, the maximum actual measurement of surface subsidence in the Haizi coal mine was only 500 mm [8], as shown in Figure 13, which indicates that the igneous sill, acting as the primary key stratum, did not break. Since the mining height was about 2.3 m, considering the geological condition of this district, it was inferred that there was at least a bed separation and fracture space of 1.5 m height developing beneath the igneous sill.

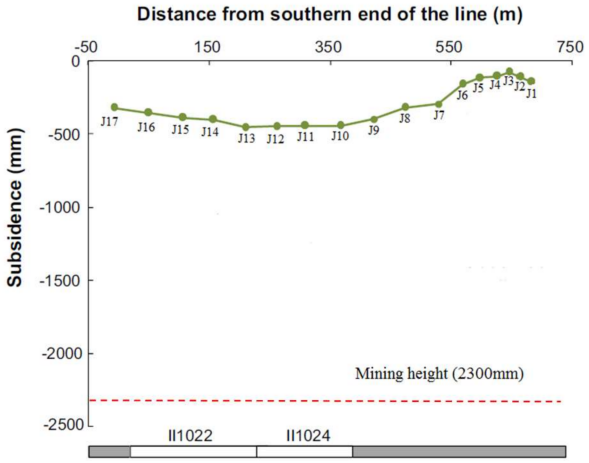

Figure 13. Investigation result of surface subsidence [8].

Dynamic disasters such as coal and gas outbursts occurred in the main gate of working face No. 1026 during the roadway advancement process. In order to weaken the threat of dynamic disaster caused by the igneous rock and to ensure the safe excavation of working face No. 1026, grouting backfilling into the overlying strata and the old goaf of working faces No. 1022 and No. 1024 was applied [28]. It was observed from the drill-hole drilling that there were some small dispersive bed separation cracks under the igneous sill, these bed separation cracks were located at 400–500 m underground and had a total height of only 500–600 mm, as shown in Figure 14. According to the above-mentioned calculations, the accumulated elastic dilatation of mining-induced unloading rock mass beneath the igneous sill is 157.9 mm. The drilling detection results together with the calculated results indicated that although the super-thick igneous sill did not break, there was no major bed separation space beneath it. Why did the major bed separation space not develop in this typical geological condition?

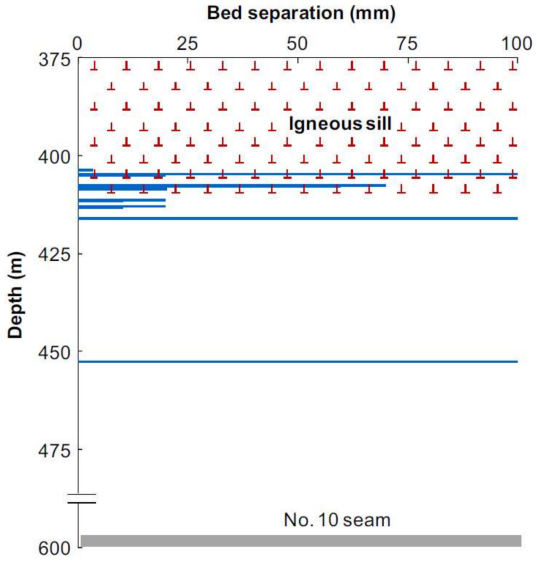

Figure 14. Detection result of bed separation [8].

According to the movement and deformation regulation of the mining-induced strata, the mining height of 2.3 m was mainly occupied by the bulking of broken rocks in the caving zone, the elastic dilatation of unloading rock mass and the bed separation between mining-induced strata in the three zones and the curving subsidence of the primary key stratum. Although the coefficient of the surface subsidence was around 1 in the nearby Linhuan coal mine and Tonglin coal mine at the full-mining stage, the super-thick igneous sill bore the load of the 400 m thick overburden, which helped the strata beneath the igneous sill to achieve full unloading and prevented the broken rocks in the caving zone from being fully compacted. Therefore, it can be concluded that uncompacted broken rocks in the caving zone was one of the significant reasons for the small bed separation space.

The estimations above were verified by the results from the drill hole after grouting for about 2 years. A drill hole D1 was drilled from the surface to working face No. 1022 to evaluate the grouting effects [29]. According to the geologic column from drill D1, the accumulated unloading dilatation of various lithological strata was calculated using the unloading elastic dilatation coefficients measured in the tests, as shown in Table 3. Parameters gained from tests on rock core in the drill column D1 were used in Equation (4), and the total compressibility of unloading rock mass due to the existence of internal load was calculated to be 18.4 mm. Then, the accumulated elastic dilatation of mining-induced unloading rock mass beneath the igneous sill in drill hole D1 was calculated to be 142.6 mm. This suggests that the elastic dilatation of mining-induced unloading rock mass beneath the super-thick igneous sill was small and as such it would have only a slight influence on the development of bed separation.

Table 3. Total amount of unloading dilatation with different lithology.

Lithology	Accumulated Thickness/m	16 MPa		32 MPa	
		Dilatation Coefficient	Dilatation/mm	Dilatation Coefficient	Dilatation/mm
Sandstone	75.62	0.90‰	68.1	1.42‰	107.4
Sand-shale	85.33	0.91‰	77.7	1.43‰	122.0
Coal	5.77	2.63‰	15.2	4.88‰	28.2
Total	166.72	/	161.0	/	257.6

This drill hole revealed the filling status of coal ash in the overlying strata as shown in Figures 15 and 16. It is obvious from Figure 16, that only 0.33 m of the total 1.67 m grouting filling thickness was

located in the fracture zone and bending zone, and the remaining 1.34 m was in the caving zone, which further indicates that the caved rock mass in the caving zone took up the most of the excavated space.

Figure 15. Picture of core-drilling.

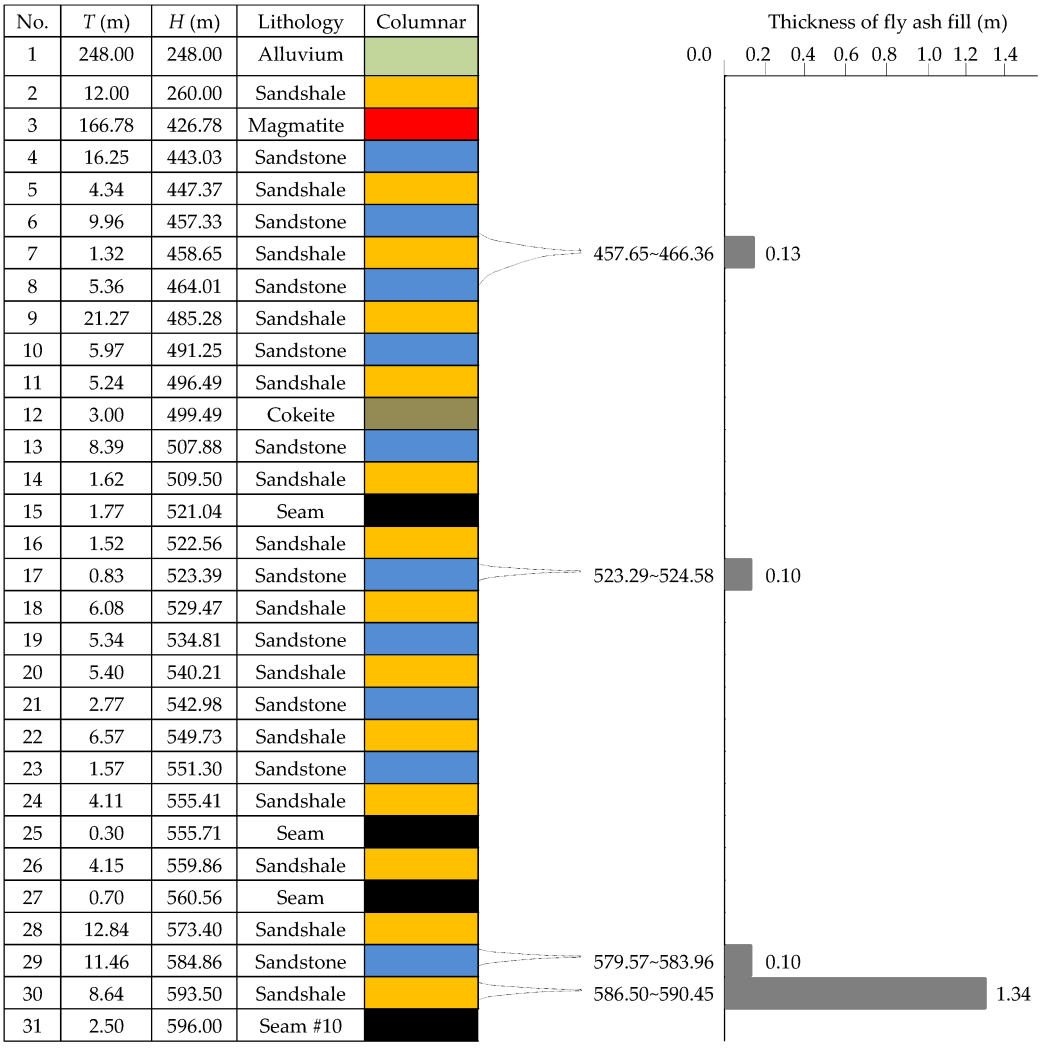

No.	*T* (m)	*H* (m)	Lithology	Columnar
1	248.00	248.00	Alluvium	
2	12.00	260.00	Sandshale	
3	166.78	426.78	Magmatite	
4	16.25	443.03	Sandstone	
5	4.34	447.37	Sandshale	
6	9.96	457.33	Sandstone	
7	1.32	458.65	Sandshale	
8	5.36	464.01	Sandstone	
9	21.27	485.28	Sandshale	
10	5.97	491.25	Sandstone	
11	5.24	496.49	Sandshale	
12	3.00	499.49	Cokeite	
13	8.39	507.88	Sandstone	
14	1.62	509.50	Sandshale	
15	1.77	521.04	Seam	
16	1.52	522.56	Sandshale	
17	0.83	523.39	Sandstone	
18	6.08	529.47	Sandshale	
19	5.34	534.81	Sandstone	
20	5.40	540.21	Sandshale	
21	2.77	542.98	Sandstone	
22	6.57	549.73	Sandshale	
23	1.57	551.30	Sandstone	
24	4.11	555.41	Sandshale	
25	0.30	555.71	Seam	
26	4.15	559.86	Sandshale	
27	0.70	560.56	Seam	
28	12.84	573.40	Sandshale	
29	11.46	584.86	Sandstone	
30	8.64	593.50	Sandshale	
31	2.50	596.00	Seam #10	

Figure 16. Columnar section and filling horizon of fly ash of drill hole D1. *T* is the thickness of each stratum. *H* is the distance from each stratum to ground.

7. Discussion of Limitations

The accumulative dilatation effect of mining-induced unloading rock mass was initially proposed in this paper, and it was preliminarily investigated based on the typical geological conditions of the Haizi coal mine. However, there are some limitations in this research and therefore some improvements are needed in future studies. These are listed as follows:

(1) Since there was only one drill hole adopted in the test for specimens and the number of specimens was limited, the value of untested specimens was estimated according to the test results of specimens with similar properties. This results in some uncertainties in the precise calculation of dilatation.

(2) The simplified stress paths in the triaxial test neglected the influence of tectonic stress in the consideration of horizontal stress. However, tectonic stress was mostly included in the in situ stress, as has been extensively indicated in numerous studies [30–32]. Furthermore, the stress variations in the rock mass induced by underground coal mining are very complex. The simplification of stress paths in this paper might bring some inaccuracies to the calculation.

(3) Due to the limitation in the number of specimens, the unloading values of all the specimens were 16/32 MPa, which slightly overestimated the dilatation coefficient of some specimens. According to the columnar section of drill hole 06-1, the depth of the bottom of igneous rock is 458.29 m. If the average unit weight is evaluated as 25 KN/m^3, the vertical in situ stress can be calculated as 11.46 MPa. For the stratum right beneath the igneous sill, the unloading stress was overestimated by $(16-11.46)/11.46 \approx 39\%$. Apparently, the result of the final calculation of the accumulated dilatation should be less than 157 mm as described above.

(4) As described in the introduction, the dynamic caving process of overlying strata has a compaction effect on the cracked rock mass in the caving zone. Hence, comprehensive consideration of cracked rock mass in the caving zone and unloading rock mass in the fracture zone and bending zone are needed in order to accurately calculate mining-induced bed separation size and surface subsidence.

Due to the limitations described above, extensive future studies are needed. The future studies should focus on how the stress in the rock mass changes due to the underground coal mining, and take tectonic stress into account, so that the sophisticated stress unloading path can be utilized. Moreover, the elastic dilatation of the rock mass in the fracture and bending zone, and the plastic dilatation of the cracked rock mass in the caving zone should be considered together to gain an accurate prediction of bed separation and surface subsidence in underground coal mining engineering. Despite its limitations, the research in this paper could still provide a good reference for future research related to dilatation of mining-induced rock mass, since this paper was the first attempt in this research area.

8. Conclusions

Underground coal mining causes stress relief and strata movement, resulting in the development of fractures and bed separation das well as ground subsidence. Understanding how strata break, fractures and bed separation develop, is of great importance for underground disaster control and sustainable mining. Based on the rules of mining-induced strata movement and stress evolution, accumulative dilatation of mining-induced unloading rock mass was proposed in this paper for the first time. The effect of the elastic dilatation of mining-induced unloading rock mass on the development of the bed separation was evaluated based on the typically geological conditions in the Haizi coal mine, China. Laboratory experiment involves a triaxial unloading test was utilized as the main tool to quantify the elastic dilatation coefficients of the rock specimens obtained from the selected drill hole in the Haizi coal mine.

The results obtained in the triaxial unloading test showed that the elastic dilatation coefficients of four unloading hard rocks and coal were 0.9~1.0‰ and 2.63‰, respectively, under the axial load of 16 MPa, and the corresponding values increased to 1.30~1.59‰ and 4.88‰ when the axial load grew to

32 MPa. It was calculated that the accumulated elastic dilatation of the 180 m thick rock mass beneath the super-thick igneous sill in the No. 102 district of the Haizi coal mine, after fully unloading to be 175.0 mm and it increased to 278.0 mm when cover depth doubled. After the successive excavation of working faces No. 1022 and No. 1024, the elastic dilatation of unloading rock mass was 157.9 mm due to the impact of the upper body load, indicating that there is a modest influence of the elastic dilatation of mining-induced unloading rock mass on the development of bed separation. Drill hole detection results after grouting showed that only 0.33 m of the total 1.67 m grouting filling thickness was located in the fracture zone and bending zone, which verified the previous drill hole detection results that indicated that only a small bed separation had developed beneath the igneous sill. Therefore, it was concluded that the influences of elastic dilatation of mining-induced unloading rock mass and bulking of caved rock mass jointly contributed to the small bed separation space beneath the igneous sill.

However, due to the limitation of the rock specimens and the simplification of the loading-unloading path, corresponding deficiencies inevitably exist in this research. Future research should use more sophisticated stress paths that consider the tectonic stress and the stress changes induced by underground mining, thereby obtaining a more accurate calculation of the dilatation of mining-induced unloading rock mass. Despite the limitations discussed above, it is reasonable to conclude that the research in this paper still could provide a good reference for future research related to the dilatation of mining-induced rock mass since this paper was the first attempt in this research area.

Acknowledgments: The financial supports provided by the State Key Research Development Program of China (2016YFC0501104) and the National Natural Science Foundation of China (51604258, 51604259) are gratefully acknowledged. The first author is also grateful to China Scholarship Council Fund (201606425074).

Author Contributions: For this paper, Weibing Zhu put forward study ideas and designed the article structure; Shengchao Yu revised the whole English writing style and discussed the design flow with Weibing Zhu; Jingmin Xu wrote the paper and analyzed the data from the mine site as well as conducting the theoretical simulation.

Conflicts of Interest: The authors declare no conflict of interest.

References

1. Qian, M.Z.; Shi, P.W.; Xu, J.L. *Ground Pressure and Strata Control*, 2nd ed.; China University of Mining and Technology Press: Xuzhou, China, 2010; pp. 66–70.
2. Qu, Q.D.; Xu, J.L.; Wu, R.L.; Qin, W.; Hu, G.Z. Three-zone characterisation of coupled strata and gas behaviour in multi-seam mining. *Int. J. Rock Mech. Min. Sci.* **2015**, *78*, 91–98. [CrossRef]
3. Sweby, G. *Review the Caving Mechanisms around High Extraction Systems and Determine the Effect of the Mechanism on the Safety of the System*; SIMRAC Project Report COL 327; CSIR Miningtek: Johannesburg, South Africa, 1997.
4. Palchik, V. Formation of fractured zones in overburden due to longwall mining. *Environ. Geol.* **2003**, *44*, 28–38.
5. Zhu, W.B.; Xu, J.M.; Li, Y.C. Mechanism of the dynamic pressure caused by the instability of upper chamber coal pillars in Shendong coalfield, China. *Geosci. J.* **2017**, *21*, 729–741. [CrossRef]
6. Zhu, W.B.; Xu, J.M.; Xu, G. Mechanism and control of roof fall and support failure incidents occurring near longwall recovery roadways. *J. South. Afr. Inst. Min. Metall.* **2017**, *117*, 1063–1072. [CrossRef]
7. Guo, H.; Yuan, L.; Shen, B.T.; Qu, Q.D.; Xue, J.H. Mining-induced strata stress changes, fractures and gas flow dynamics in multi-seam longwall mining. *Int. J. Rock Mech. Min. Sci.* **2012**, *54*, 129–139. [CrossRef]
8. Xuan, D.Y.; Xu, J.L.; Zhu, W.B. Dynamic disaster control under a massive igneous sill by grouting from surface boreholes. *Int. J. Rock Mech. Min. Sci.* **2014**, *71*, 176–187. [CrossRef]
9. Ju, J.F.; Xu, J.L. Surface stepped subsidence related to top-coal caving longwall mining of extremely thick coal seam under shallow cover. *Int. J. Rock Mech. Min. Sci.* **2015**, *78*, 27–35. [CrossRef]
10. Zhu, W.B.; Xu, J.M.; Xu, J.L.; Chen, D.Y.; Shi, J.X. Pier-column backfill mining technology for controlling surface subsidence. *Int. J. Rock Mech. Min. Sci.* **2017**, *96*, 58–65. [CrossRef]
11. Suorineni, F.T. Editorial. *J. Rock Mech. Geotech. Eng.* **2015**, *7*, 481–482. [CrossRef]
12. Su, Z.J. Research of Deformation Mechanism of Mining Overburden Separated Strata. Ph.D. Thesis, Liaoning Technical University, Fuxin, China, 2001.

13. Zhang, W.; Zheng, J.F.; Yu, G.M.; Xu, Y.Y.; Zhang, C.H. Research on mechanical criterion of formation of separation layer in cover rock. *Rock Soil Mech.* **2006**, *27*, 275–278.
14. Jiang, Y. The bed-separated zone and its distribution law in the overlying strata affected by mining. *J. Shandong Min. Inst.* **1997**, *16*, 19–22.
15. Li, S.G. Calculate the equivalent area of overlying strata bed separated fissures before and after rupture of the key stratum. *J. Xi'an Min. Inst.* **1999**, *19*, 289–292.
16. Tibbett, J.D.; Suorineni, F.T.; Hebblewhite, B.K. Preliminary investigation of rock mass response to undercut blasting in a block cave mining system using virtual reality scientific visualisation. *CIM J.* **2016**, *7*, 121–131. [CrossRef]
17. Xuan, D.Y.; Xu, J.L. Grout injection into bed separation to control surface subsidence during longwall mining under villages: Case study of Liudian coal mine, China. *Nat. Hazards* **2014**, *73*, 883–906. [CrossRef]
18. Xing, M.L.; Li, W.P.; Wang, Q.Q.; Yang, D.D. Risk prediction of roof bed-Separation water inrush in a coal mine, China. *Electron. J. Geothechnical Eng.* **2015**, *20*, 301–312.
19. Vukelič, Ž.; Dervarič, E.; Šporin, J.; Vižintin, G. The development of dewatering predictions of the Velenje coalmine. *Energies* **2016**, *9*, 702. [CrossRef]
20. Qian, M.G.; Miao, X.X.; Xu, J.L.; Mao, X.B. *Study of Key Strata Theory in Ground Control*; China University of Mining and Technology Press: Xuzhou, China, 2002; pp. 16–20.
21. Xu, J.L.; Qian, M.G.; Jin, H.W. Study and application of bed separation distribution and development in the process of strata movement. *Chin. J. Geotech. Eng.* **2004**, *26*, 632–636.
22. Miao, X.X.; Mao, X.B.; Hu, G.W. Research on broken expand and press solid characteristics of rocks and coals. *J. Exp. Mech.* **1997**, *12*, 394–400.
23. Guo, G.L.; Miao, X.X.; Zhang, Z.N. Research on ruptured rock mass deformation characteristics of longwall goofs. *Sci. Technol. Eng.* **2002**, *2*, 44–47.
24. Jiang, Z.Q.; Ji, L.J.; Zuo, R.S. Research on mechanism of crushing compression of coal waste. *J. China Univ. Min. Technol.* **2001**, *30*, 139–142.
25. Salamon, M.D.G. Mechanism of Caving in Longwall Mining. Rock Mechanics Contributions and Challenges. In Proceedings of the 31st US Symposium on Rock Mechanics, Golden, CO, USA, 18–20 June 1990; pp. 161–169.
26. Su, C.D.; Gu, M.; Tang, X.; Guo, W.B. Experiment study of compaction characteristics of crushed stones from coal seam roof. *Chin. J. Rock Mech. Eng.* **2012**, *31*, 18–26.
27. Cai, M.; Kaiser, P. Visualization of rock mass classification systems. *Geotech. Geol. Eng.* **2006**, *24*, 1089–1102. [CrossRef]
28. Xuan, D.Y.; Xu, J.L.; Zhu, W.B.; Wang, L. Field test on dynamic disaster control by grouting below extremely thick igneous rock. *J. China Coal Soc.* **2012**, *37*, 1967–1974.
29. Wang, B.L.; Xu, J.L.; Liu, K.; Xuan, D.Y. Study on grouting and backfill effect of drilling exploration under ultra thick igneous rock. *Coal Sci. Technol.* **2014**, *42*, 25–27.
30. Li, T.; Cai, M.F.; Cai, M. A review of mining-induced seismicity in China. *Int. J. Rock Mech. Min. Sci.* **2007**, *44*, 1149–1171. [CrossRef]
31. Vižintin, G.; Mayer, J.; Lajlar, B.; Vukelič, Ž. Rock burst dependency on the type of steel arch support in the Velenje mine. *Mater. Tehnol.* **2017**, *51*, 11–18. [CrossRef]
32. Vižintin, G.; Kocjančič, M.; Vulić, M. Study of coal burst source locations in the Velenje colliery. *Energies* **2016**, *9*, 507. [CrossRef]